



Cite this: *Phys. Chem. Chem. Phys.*,  
2018, 20, 13316

# Revealing the linear relationship between electrical, thermal, mechanical and structural properties of carbon nanocoils

Chenghao Deng,<sup>a</sup> Chengwei Li,<sup>a</sup> Peng Wang,<sup>a</sup> Xinwei Wang<sup>id</sup><sup>b</sup> and Lujun Pan<sup>id</sup><sup>\*a</sup>

The special helical morphologies and polycrystalline–amorphous internal structures differ carbon nanocoils (CNCs) from carbon nanotubes or carbon nanofibers, but bring difficulties in illuminating the correlations between physical and structural properties. In this paper, we measure the electrical conductivity ( $\sigma$ ), thermal diffusivity ( $\alpha$ ) and Young's modulus ( $E$ ) of single CNCs at the same time, using a transient electrothermal technique and an electromechanical vibration technique. Based on the statistical results of 8 single CNC samples, a linear correlation between the three parameters is uncovered, expressed as  $\sigma = 0.052(\alpha - 2.5) \times 10^4 \text{ S m}^{-1}$ ,  $E = (-10.38\sigma + 14.04) \text{ GPa}$  and  $E = (-0.59\alpha + 16.08) \text{ GPa}$ , where the unit of  $\alpha$  is  $10^{-7} \text{ m}^2 \text{ s}^{-1}$ . Concise proportional relations between the three parameters and average graphite grain size ( $l_d$ ) are deduced, expressed as  $\sigma = A l_d (C_1 - T)^{-1}$ ,  $\alpha = B l_d (C_2 + T)^{-1}$  and  $E = -D l_d + E_0$ . The proportional relation between physical parameters and  $l_d$  demonstrates the confinement originated from the nano-grain system.

Received 1st March 2018,  
Accepted 13th April 2018

DOI: 10.1039/c8cp01349g

rsc.li/pccp

## 1. Introduction

Carbon nanocoils (CNCs) are quasi 1-dimensional carbon nanomaterials with unique helical morphology.<sup>1,2</sup> They show potential applications in field emitters,<sup>3,4</sup> reinforcing materials for composites,<sup>5</sup> infrared sensors,<sup>6</sup> wave absorbers,<sup>7</sup> strain sensors,<sup>8</sup> self-sensing mechanical resonators,<sup>9</sup> etc. Nowadays, the most widely adopted synthesis method of CNCs is chemical vapor deposition (CVD),<sup>10–13</sup> which can control the growth of CNCs by changing catalysts and CVD conditions. The formation of coils is a result of different carbon precipitation rates on different faces of a polyhedron catalyst particle. It is noted that the CVD synthesized CNCs have a special polycrystalline–amorphous internal structure.<sup>10,14,15</sup>  $sp^2$  Bonded graphite nano-grains are embedded in an  $sp^3$  bonded amorphous carbon matrix.<sup>16</sup> The average grain size of graphite in CNCs is around 3.5 nm.<sup>17</sup> Chen *et al.* measured the ratio of  $sp^2$  to  $sp^3$  structures in CNCs to be 4:1 by electron energy loss spectroscopy.<sup>18</sup> Although the grain size is so small, the  $sp^2$  graphite grain is the dominated structure, differing CNCs from amorphous carbon nanofibers (CNFs). The physical properties of CNCs depend strongly on the size and arrangement of  $sp^2$  graphite grains. Many efforts have been made to

investigate the electrical, thermal and mechanical properties of CNCs.

The electrical conductivities of CNCs are determined by the hopping barrier (thermal activation energy) between graphite grains. The room temperature (RT) electrical conductivity of CNCs ranges from 20 to 200  $\text{S cm}^{-1}$ .<sup>15,19</sup> Ma *et al.* studied the annealing effect on the electrical properties of CNCs.<sup>20</sup> With annealing temperature ( $T$ ) increasing from 973 to 1273 K, the resistivity decreases sharply from  $1.9 \times 10^{-4}$  to  $7.7 \times 10^{-5} \Omega \text{ m}$ , with a hopping barrier decreasing from 11 to 4.2 meV. The average grain size was increased from 4.3 to 14 nm accompanied by the reduction of amorphous structures between grains. With the increase of crystallinity, the coherence of grains also gets better. With the decrease of temperature, the electron transport in CNCs experiences three stages with different dominated conduction mechanisms, from nearest-neighbor hopping to Efros–Shklovskii variable range hopping.<sup>15</sup>

Owing to the polycrystalline–amorphous structure, CNCs exhibit quite different phonon behavior compared to amorphous CNFs or multi-walled carbon nanotubes (CNTs).<sup>21,22</sup> Their RT thermal conductivity ( $\kappa$ ) ranges from 1.6 to 38  $\text{W m}^{-1} \text{ K}^{-1}$ .<sup>17,23,24</sup> The  $\kappa$ – $T$  curve of CNCs shows a peak around 75 K, and the specific heat– $T$  curve also shows a shoulder at 75 K. For CNTs with good crystallinity, this feature temperature is much higher (always higher than 400 K), and amorphous carbon does not have this feature temperature.<sup>25</sup> Deng *et al.* used the reciprocal of thermal diffusivity (called thermal reffusivity) to evaluate the domain size of CNCs.<sup>17</sup> It was found that the thermal

<sup>a</sup> School of Physics, Dalian University of Technology, Ganjingzi District,  
No. 2 Linggong Road, Dalian 116024, P. R. China. E-mail: lpan@dlut.edu.cn

<sup>b</sup> Department of Mechanical Engineering, Iowa State University,  
2010 Black Engineering Building, Ames, IA 50011, USA

recessivity–temperature curve of CNCs is linear, which differs from the exponential curve of graphite or graphene. This difference was attributed to the  $sp^2/sp^3$  hybrid structure. The scattering from the amorphous matrix and grain boundary plays a crucial role in the phonon transport in CNCs.

Due to the helical morphology, the mechanical properties of CNCs show the most intuitive difference compared to other carbon nanomaterials. The torsion dominates the total strains of CNCs with a deformation.<sup>18,26,27</sup> Even if CNCs are helical multi-walled CNTs with good crystallinity, the mechanical response is quite different from that of CNTs. The mechanical response of CNCs is determined by the slide of graphite layers, while that of CNTs is determined by the in-plane stretch of the hexatomic ring. This difference leads to the negative correlation between crystallinity and shear modulus of CNCs. The Young's modulus of CNCs ranges from 2 to 200 GPa, depending strongly on their crystallinities.<sup>27–30</sup>

Unlike CNTs, the physical properties of polycrystalline–amorphous CNCs cannot be well predicted through theory or numerical calculation. From a physical point of view, the electrical, thermal and mechanical properties of a CNC must be correlated, determined by its internal structure. It is of great significance to figure out how the interactions between graphite grains and the amorphous matrix in a CNC affect the electron and phonon transportations and its mechanical strength. Despite the numerous studies of the physical properties of CNCs, the effect of the polycrystalline–amorphous structure is still unclear. In this paper, we measured the RT thermal diffusivity, electrical conductivity and Young's modulus of single CNCs and obtained statistical data which showed the relation between these characteristic constants.

## 2. Experimental

### 2.1. Synthesis of CNCs by chemical vapor deposition (CVD)

The CNCs were synthesized using a CVD method.  $0.2 \text{ mol L}^{-1}$  solution consisting of  $\text{Fe}_2(\text{SO}_4)_3 \cdot 9\text{H}_2\text{O}$ ,  $\text{SnCl}_2 \cdot 5\text{H}_2\text{O}$  and deionized water was used as the catalyst precursor. The catalyst was first dipped in the quartz substrate and then calcined at  $710^\circ\text{C}$  for 30 min in an argon atmosphere with an Ar flow rate of 365 sccm. At last, the carbon deposits were obtained at  $710^\circ\text{C}$  for 1 h by introducing acetylene and argon gases with flow rates of 15 and 325 sccm, respectively.

### 2.2. Electrical conductivity and thermal diffusivity measurements

The thermal diffusivity and electrical conductivity of single CNCs were measured using a transient electrothermal technique (TET). The TET is an effective method for measuring the thermophysical properties of 1-dimensional conductive and nonconductive micro/nanoscale materials, which was developed by Wang *et al.*<sup>31–33</sup> A single CNC was suspended between two gold electrodes using silver paste, with the help of micro tungsten probes under an optical microscope. The scanning electron microscope (SEM) image of a typical suspended CNC

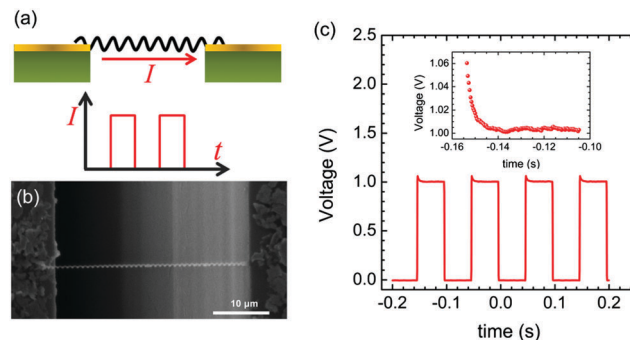


Fig. 1 (a) Schematic of TET tests. (b) SEM image of a typical single CNC sample. (c) Voltage evolution recorded using an oscilloscope. The inset is an enlarged vision for one top edge.

sample is shown in Fig. 1b. Then a step current was fed onto the single CNC, whose value ranged from 1 to  $3 \mu\text{A}$ , as shown in Fig. 1a. The experiment was conducted in a vacuum chamber with air pressure smaller than 1 Pa. Single CNCs were heated by joule heating. In the vacuum chamber, CNCs show two ways of heat dissipation, which are heat conduction along the length direction and thermal radiation. The thermal radiation can be neglected compared to heat conduction.<sup>17</sup> As the resistance of a CNC decreases with increasing temperature, there is a resistance evolution process until thermal equilibrium is achieved. An oscilloscope was employed to monitor the voltage evolution (same as resistance evolution when the current was fixed). Fig. 1c shows the voltage evolution curve of a CNC sample. The inset in Fig. 1c is an enlarged vision for one top edge. Using a Matlab fitting program, thermal diffusivity was obtained from the voltage evolution curve. A detailed principle for suspended CNC sample preparation and TET tests can be found in our previous work.<sup>17</sup>

### 2.3. Young's modulus measurements

The Young's modulus of single CNCs was measured using an electromechanical vibration technique. Detailed principles can be found in our previous work.<sup>27</sup> The suspended CNC sample was cut off at root by a focused laser, obtaining a CNC cantilever. Then a microprobe was employed as a counter electrode, forming a capacitor structure. An alternative voltage and a bias voltage, with values of 10 V and 30 V respectively, were applied to them, as shown in Fig. 2a. The CNC cantilever was driven to

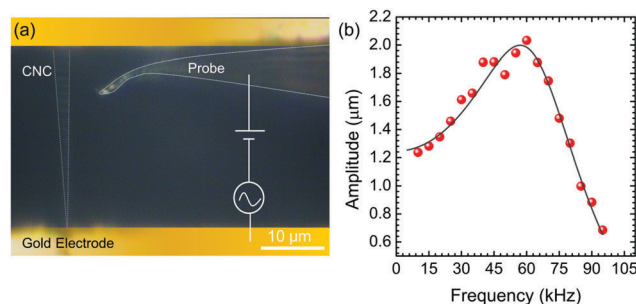


Fig. 2 (a) CCD image of electromechanical vibration of a typical CNC sample. (b) Amplitude–frequency curve of a CNC sample.

vibrate by the alternative static electrical forces. Fig. 2b presents the amplitude–frequency relation of a typical CNC's vibration. A fitting function deduced from the classical continuum model was used to fit the amplitude–frequency relation curve and obtain the resonance frequency. Then we can calculate the Young's modulus from the resonance frequency through a material mechanics based formula.<sup>27</sup> The resonance frequency in Fig. 2b is fitted to be 68 kHz.

### 3. Results and discussion

Fig. 3 shows the TEM image of (a) a typical CNC, and (b) its high resolution TEM image. CNCs are hollow inside and have a highly disordered structure. Fig. 5a shows a higher resolution TEM image of CNCs. On the whole, the internal structure of carbon nanocoils is similar to a jujube cake. Graphite nanograins are embedded in an amorphous matrix. The difference in the scale of graphite grains is larger than that of the amorphous space between grains. The spaces between graphite nanograins are essentially defects of a perfect graphite structure, which are hybrids of vacancies and  $sp^3$  bonded carbons, such as  $-COO-$ ,  $-CO-$  and  $-C-C-$ .<sup>34</sup> Graphite grains are connected through covalent bonds or intermolecular forces of some functional groups, such as  $-COOH$ ,  $-CH_x$  or  $-COH$ . The crystallinity of CNCs was evaluated using Raman spectra, one of which is shown in the inset of Fig. 3a. The average size of  $sp^2$  graphite grains for the CNC in Fig. 3a is calculated to be 4.26 nm, using an empirical formula:  $I_D/I_G = C(\lambda)/L_a$ , where  $C(\lambda) = 12.6 + 0.033\lambda$  (nm).<sup>35</sup> The main orientation of  $sp^2$  grains can be observed from the electron diffraction pattern in the inset of Fig. 3b. The arc-shaped diffraction pattern corresponds to the (002) lattice plane of graphite, and the interplanar spacing is calculated to be 0.352 nm.

The graphitization degree of CNCs differs from sample to sample, which leads to different physical properties for these CNCs. Fig. 4 presents the simple correlation between thermal diffusivity, electrical conductivity and Young's modulus of 8 single CNC samples. Fig. 4a shows the linear relationship between thermal diffusivity ( $\alpha$ ) and electrical conductivity ( $\sigma$ ):  $\sigma = 0.052(\alpha - 2.5) \times 10^4 \text{ S m}^{-1}$ , where the unit of  $\alpha$  is  $10^{-7} \text{ m}^2 \text{ s}^{-1}$ . The 2.5 offset of  $\alpha$  means: when CNC becomes an insulating material ( $\sigma = 0$ ), the phonon transport is still effective, different from a common metal whose heat conduction is governed by electrons. Using the offset of  $\alpha$  and specific heat obtained in

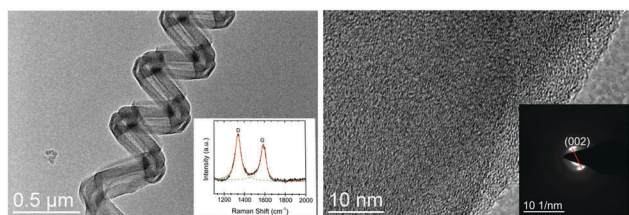


Fig. 3 (a) TEM image of a typical CNC. The inset in (a) is the Raman spectrum of the CNC. (b) Enlarged TEM image of the CNC in (a). The inset in (b) is the electron diffraction pattern of the CNC.

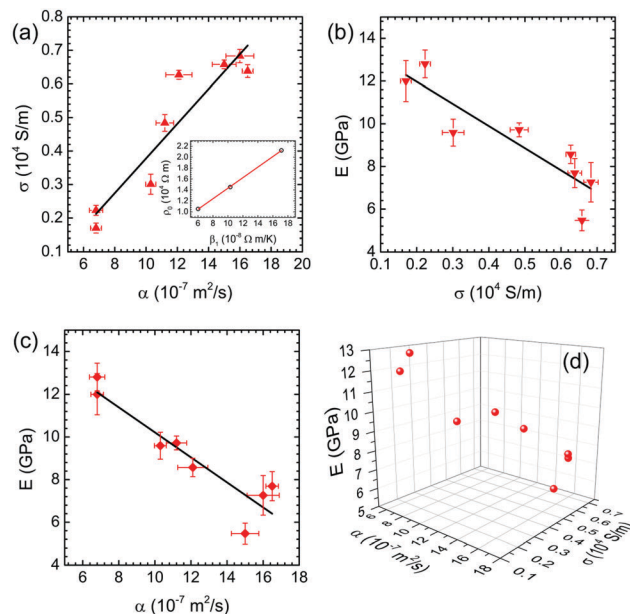


Fig. 4 Relationships between (a) electrical conductivity and thermal diffusivity, (b) Young's modulus and electrical conductivity, (c) Young's modulus and thermal diffusivity. (d) Three-dimensional views between the three parameters. The inset in (a) is the linear relation between the slope and the intercept of the resistivity–temperature curve for CNC samples.

ref. 17, the smallest thermal conductivity of a CNC at RT is calculated to be  $0.5 \text{ W m}^{-1} \text{ K}^{-1}$ . This value is similar to that of amorphous carbon.<sup>36,37</sup> As shown in Fig. 5c, owing to the nanocrystalline structure, the  $sp^2$  grain performs as a domain or a localized state. The electron and phonon transports in a graphite grain are almost unimpeded, but are scattered by the boundary of grains and the amorphous structures between grains. As we know, the  $sp^3$  bonded carbons cannot transport electrons. The electron hopping between  $sp^2$  grains in a carbon nanocoil has been demonstrated.<sup>38</sup> Similarly, the phonon transport will also

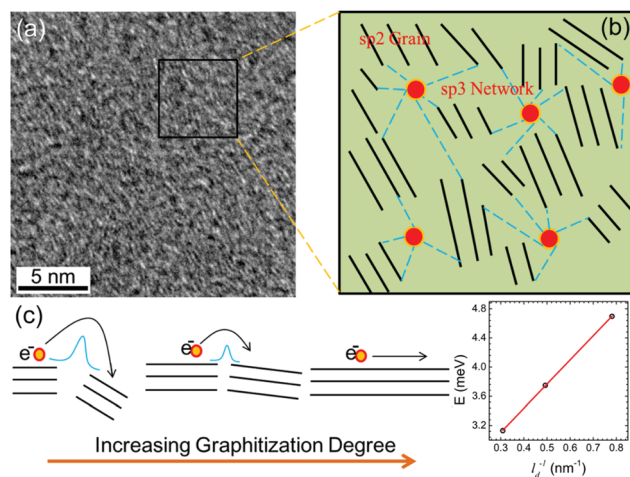


Fig. 5 (a) TEM image and (b) schematic view of internal structures of CNCs. (c) Schematic illustration of electron hopping and the inversely linear relation between the hopping barrier and  $sp^2$  grain size.

be impeded by the amorphous structure. That is, the electron and phonon transports are all determined by the scale of the amorphous matrix, or the size of the grain relatively, which may result in a linear relation between  $\alpha$  and  $\sigma$ .

The electrical conductivity of CNCs can be expressed as  $\sigma = n(T)e\mu(T)$ , where  $n$  is the concentration of conduction electrons, and  $\mu$  is the mobility which is determined by scattering effects. Compared to the electron concentration, the change of  $\mu(T)$  with temperature is very small. Here, we only consider the change of  $n(T)$  like the other methods reported in ref. 14 and 15. Due to the highly disordered structure, the electron transport in CNCs is explained by an electron hopping mechanism. Electrons would hop from one localized state to another, overcoming a hopping barrier, as shown in Fig. 5c. Thus, the concentration of conduction electrons  $n$  is determined by the hopping barrier and temperature.  $n$  is expressed as  $n_0e^{(-E/KT)}$ , where  $n_0$ ,  $E$ ,  $K$  and  $T$  are the initial concentration of electrons, the hopping barrier, the Boltzmann constant and temperature, respectively. Combining the analysis mentioned above with the experimental results reported, the electrical conductivity  $\sigma$  of CNCs can be described as

$$\frac{1}{\sigma} = \rho_i + \rho_s e^{E/KT} \quad (1)$$

where  $\rho_i$  and  $\rho_s$  are the constants related to the internal structures of CNCs.  $\rho_i$  represents a residual resistance.  $1/\rho_s$  represents the concentration of free electrons in an  $sp^2$  grain.

The thermal diffusivity  $\alpha$  of CNCs is determined by the scattering effect, which is expressed as  $\alpha = \nu^2\tau/3$ , where  $\nu$  and  $\tau$  are the average phonon velocity and the relaxation time of phonon transport.  $\tau$  is determined by scattering effects of phonons. According to the Matthiessen rule,<sup>39</sup> it is generally a good approximation to linearly add all the scattering effects for the overall scattering effect. Therefore,  $\tau$  can be expressed as

$$\frac{1}{\tau} = \frac{1}{\tau_U} + \frac{1}{\tau_{\text{boundary}}} + \frac{1}{\tau_{\text{defects}}} \quad (2)$$

where  $\tau_U$ ,  $\tau_{\text{boundary}}$  and  $\tau_{\text{defects}}$  are the relaxation time corresponding to Umklapp-scattering, boundary and defect scattering, respectively.  $\tau_U$  increases exponentially with temperature while  $\tau_{\text{defects}}$  and  $\tau_{\text{boundary}}$  are only related to the internal structures.

Then, the thermal diffusivity  $\alpha$  of CNCs is expressed as

$$\frac{1}{\alpha} = \frac{3}{\nu^2} \left( \frac{1}{\tau_0} + \frac{1}{\tau_U} \right) \quad (3)$$

where  $1/\tau_0$  is the sum of  $1/\tau_{\text{defects}}$  and  $1/\tau_{\text{boundary}}$ . The expression of  $\tau_U$  is given as  $\tau_U = \tau_s e^{\theta_D/2T}$ , where  $\theta_D$  is the Debye temperature of CNCs.<sup>40</sup>  $\tau_s$  is a constant corresponding to an initial relaxation time. The product of  $\tau_0$  and  $\nu$  corresponds to the size of  $sp^2$  grains ( $l_0 = \tau_0\nu$ ).

Then the expression of  $\alpha$  is written as

$$\frac{1}{\alpha} = \frac{3}{\nu l_0} + \frac{3}{\nu l_s} e^{-\theta_D/2T} \quad (4)$$

where  $l_s = \tau_s\nu$ . Actually, the experimental results suggest a much simpler expression of electrical conductivity and thermal

diffusivity,<sup>15,17,20</sup> which are expressed as

$$\begin{aligned} \frac{1}{\sigma} &= \rho_0 - \beta_1 T \\ \frac{1}{\alpha} &= \Theta_0 + \beta_2 T \end{aligned} \quad (5)$$

where  $\Theta_0$ ,  $\rho_0$ ,  $\beta_1$  and  $\beta_2$  are four fitting coefficients. To transform eqn (1) and (4) to (5), we employ approximate Taylor expansion to the exponential term, and obtain the expressions of  $\sigma$  and  $\alpha$  as

$$\begin{aligned} \frac{1}{\sigma} &\approx \rho_0 - \rho_s \frac{K}{E} T \\ \frac{1}{\alpha} &\approx \frac{3}{\nu l_d} + \frac{6}{\nu l_s \theta_D} T \end{aligned} \quad (6)$$

The items in eqn (6) correspond to the items in eqn (5) one to one.  $l_d$  is the real grain size of CNCs. It is found from eqn (6) that larger  $E$  and smaller  $\theta_D$  determine smaller  $\sigma$  and  $\alpha$ . It is reasonable to speculate that the linear relationship between thermal diffusivity and electrical conductivity of CNCs exists in a wide temperature range, not just around RT.

The relation between  $\alpha$  and  $\sigma$  is described as

$$\sigma = k\alpha - \sigma_0 \approx k\alpha \quad (7)$$

Because  $\sigma_0$  is much smaller than  $\sigma$ , here we neglect it for simplicity.

By combining eqn (5) with (7) the following formula is deduced as

$$k = \frac{(\Theta_0 + \beta_2 T)}{(\rho_0 - \beta_1 T)} \quad (8)$$

where  $\Theta_0$ ,  $\rho_0$ ,  $\beta_1$  and  $\beta_2$  are all determined by internal structures of CNCs. As the linear relation between  $\alpha$  and  $\sigma$  exists in a wide temperature range,  $k$  should be correlated with temperature but is independent of internal structures.

Thus,  $\Theta_0$  and  $\beta_2$ ,  $\rho_0$  and  $\beta_1$  are correlated with a constant independent of internal structures, expressed as,

$$\Theta_0 = C_2\beta_2$$

$$\rho_0 = C_1\beta_1$$

where  $C_2$  and  $C_1$  are two constants. Then,  $k = \gamma \frac{(C_2 + T)}{(C_1 - T)}$ , where  $\gamma = \beta_2/\beta_1$ , which is a constant parameter to ensure that  $k$  is independent of internal structures. This result is similar to the Weidmann–Franz law, which demonstrates that the ratio of thermal conductivity to electrical conductivity of metal is proportional to temperature. The values of  $E$ ,  $\beta_1$  and  $\rho_0$  were obtained from the resistance– $T$  curve.<sup>17</sup> Then the linear relationship between  $\beta_1$  and  $\rho_0$  was revealed, as shown in the inset of Fig. 4a.

As described in eqn (6),  $\Theta_0$  is inversely proportional to the size of  $sp^2$  grains ( $l_d$ ), as  $\Theta_0 = 3/\nu l_d$ . Therefore,  $\Theta_0$ ,  $\beta_2$ ,  $\beta_1$  and  $\rho_0$  are all inversely proportional to  $l_d$ . For CNCs with a larger grain size, their electrical resistivity and thermal reffusivity

(reciprocal of thermal diffusivity) at 0 K limit are smaller, and the changes of  $1/\alpha$  and  $1/\sigma$  with temperature are also smaller, as inferred from eqn (5). Due to their nanosize,  $sp^2$  grains can be treated as quantum dots, which changes electron configuration and the concentration of free electrons in a grain. On the other hand, the hopping barrier changes with grain size. Defining  $\sigma_s$  as  $1/\rho_s$ ,  $\sigma_s$  represents the concentration of free electrons in a grain. Due to the 2D quantum confinement effect in the in-plane direction,  $\sigma_s$  may be proportional to  $l_d^2$ , determining  $E$  to be proportional to  $l_d^{-1}$ . The linear correlation between  $E$  and  $l_d^{-1}$  is presented in Fig. 5c. This linear relation can be explained by a simple tunneling model between two nanoparticles. The tunneling barrier (hopping barrier in this paper) is proportional to the distance between two particles. From three dimensional views, the internal structures of carbon nanocoils have two limiting cases, either all graphite or all amorphous structure. Thus, it is reasonable to consider that the scale of amorphous space between grains is inversely proportional to the size of grains, which determines the inverse proportion between  $E$  and  $l_d$ . From the observation of specific heat- $T$  curves for the three CNC samples in ref. 17, there is no significant difference in  $\theta_D$  for CNCs with different crystallinities. This evaluation indicates a linear relation between  $l_s$  and  $l_d$ . Now simpler expressions of  $\sigma$  and  $\alpha$  are obtained as

$$\begin{aligned}\sigma &= Al_d(C_1 - T)^{-1} \\ \alpha &= Bl_d(C_2 + T)^{-1}\end{aligned}\quad (9)$$

Fig. 4b and c show the linear relationship between  $\sigma$  and Young's modulus ( $E$ ),  $\alpha$  and  $E$ , given as

$$E = (-10.38\sigma + 14.04) \text{ GPa}$$

and

$$E = (-0.59\alpha + 16.08) \text{ GPa}$$

As  $E$  changes slowly with temperature and  $\sigma$  or  $\alpha$  is proportional to  $l_d$ , here we only consider  $E$  as a function of  $l_d$ , expressed as

$$E = -Dl_d + E_0 \quad (10)$$

The Young's modulus of polycrystalline-amorphous CNCs is strongly related to the size and arrangement of  $sp^2$  grains. Kelly proposed a model based on the stiffness of micro-graphite grains.<sup>41</sup> Under stress, the graphite layers in a grain are first slipped, producing shear deformation. Then the shear deformation of micro-grains leads to the overall deformation of graphite. For neutron irradiated polycrystalline graphite, the Young's modulus is increased several times. The irradiation induced defect is considered as a pinning site, impeding the slide of the graphite layer in a micro-grain. For nano-crystalline structured CNCs, the  $sp^3$  carbon network may also perform as a pinning center, as schematically shown in Fig. 5b. The covalent bonds of  $sp^3$  bonded carbons and intermolecular forces of functional groups enhance the internal friction between graphite grains, impeding the slide of grains and graphite layers in

a grain. The magnitude of the pinning effect may show negative linear relation to the distance between pinning centers, or the size of  $sp^2$  grains in other words, which accounts for the linear expression of eqn (10).

Previous studies have revealed the positive relation between the graphitization degree and electrical conductivity (thermal diffusivity), and the negative relation between the graphitization degree and Young's modulus.<sup>15,17,30</sup> In this work, we present a simpler and more visualized view of the relation between these parameters. All the parameters are linked to  $sp^2$  grain size. Due to the tiny size, the boundaries of  $sp^2$  grains perform as localized states, which hinder the transport of electrons and phonons and determine the boundary scattering and the hopping barrier.  $sp^3$  structures surrounding  $sp^2$  grains perform as pinning centers, binding  $sp^2$  grains together. The average distance between the pinning centers is proportional to the average size of  $sp^2$  grains. When the distance increases, shear deformation of  $sp^2$  grains becomes easier, reducing the elastic modulus of CNCs as a result. That is, all the parameters are determined by the average size of  $sp^2$  grains, giving the linear relation among thermal diffusivity, electrical conductivity and Young's modulus. The simple relation discovered in this work provides a feasible way to evaluate the physical performance of CNCs for practical applications.

## 4. Conclusion

Using a TET technique and an electromechanical vibration technique, the electrical conductivity, thermal diffusivity and Young's modulus of single CNC samples were obtained at the same time. Based on the statistical results of 8 CNC samples, we obtained simple but significant relations among the three parameters, expressed as  $\sigma = 0.052(\alpha - 2.5) \times 10^4 \text{ S m}^{-1}$ ,  $E = (-10.38\sigma + 14.04) \text{ GPa}$  and  $E = (-0.59\alpha + 16.08) \text{ GPa}$ , where the unit of  $\alpha$  is  $10^{-7} \text{ m}^2 \text{ s}^{-1}$ . Furthermore, we deduced concise proportional relations between physical parameters and grain size, described by  $\sigma = Al_d(C_1 - T)^{-1}$ ,  $\alpha = Bl_d(C_2 + T)^{-1}$  and  $E = -Dl_d + E_0$ . As the localized state and the quantum dot,  $sp^2$  grains play an important role in electron and phonon transportation. The amorphous networks between  $sp^2$  grains acting as pinning centers impede the shear deformation of  $sp^2$  grains. It is the special internal structures of CNCs that determine their special physical behaviors and the linear relations among these physical parameters.

## Conflicts of interest

There are no conflicts of interest to declare.

## Acknowledgements

This work was supported by the National Natural Science Foundation of China (No. 51661145025, 11274055, 61520106013)

## References

- 1 S. Ihara, S. Itoh and K. Ji, *Phys. Rev. B: Condens. Matter Mater. Phys.*, 1993, **48**, 5643.
- 2 S. Amelinckx, X. B. Zhang, D. Bernaerts, X. F. Zhang, V. Ivanov and J. B. Nagy, *Science*, 1994, **265**, 635.
- 3 L. Pan, T. Hayashida, M. Zhang and Y. Nakayama, *Jpn. J. Appl. Phys.*, 2001, **40**, L235–L237.
- 4 L. Pan, Y. Konishi, H. Tanaka, O. Suekane, T. Nosaka and Y. Nakayama, *Jpn. J. Appl. Phys.*, 2005, **44**, 1652–1654.
- 5 K. Sanada, Y. Takada, S. Yamamoto and Y. Shindo, *Journal of Solid Mechanics and Materials Engineering*, 2008, **2**, 1517–1527.
- 6 H. Ma, L. Pan, Q. Zhao and W. Peng, *Nanoscale*, 2013, **5**, 1153.
- 7 U. Eguchi, H. Takikawa and Y. Suda, *Jpn. J. Appl. Phys.*, 2014, **53**, 205–211.
- 8 C. Li, L. Pan, C. Deng and P. Wang, *RSC Adv.*, 2016, **6**.
- 9 A. Volodin, B. Dieter, A. Markus and F. Antonio, *Nano Lett.*, 2004, **4**, 1775–1779.
- 10 N. Tang, W. Kuo, C. Jeng, L. Wang, K. Lin and Y. Du, *ACS Nano*, 2010, **4**, 781.
- 11 E. X. Ding, J. Wang, H. Z. Geng, W. Y. Wang, Y. Wang, Z. C. Zhang, Z. J. Luo, H. J. Yang, C. X. Zou and J. Kang, *Sci. Rep.*, 2015, **5**, 11281.
- 12 J. Sun, A. A. Koós, F. Dillon, K. Jurkschat, M. R. Castell and N. Grobert, *Carbon*, 2013, **60**, 5–15.
- 13 R. Cui, L. Pan and C. Deng, *Carbon*, 2015, **89**, 47–52.
- 14 H. S. Chiu, P. I. Lin, H. C. Wu, W. H. Hsieh, C. D. Chen and Y. T. Chen, *Carbon*, 2009, **47**, 1761–1769.
- 15 Y. Sun, C. Wang, L. Pan, X. Fu, P. Yin and H. Zou, *Carbon*, 2016, **98**, 285–290.
- 16 Q. Zhao, L. J. Pan, H. Ma and T. Wang, *Diamond Relat. Mater.*, 2012, **22**, 33–36.
- 17 C. Deng, Y. Sun, L. Pan, T. Wang, Y. Xie, L. Jing, B. Zhu and X. Wang, *ACS Nano*, 2016, **10**.
- 18 X. Chen, S. Zhang, D. A. Dikin, A. Weiqiang Ding, R. S. Ruoff, L. P. And and Y. Nakayama, *Nano Lett.*, 2003, **3**, 1299–1304.
- 19 T. Hayashida, L. Pan and Y. Nakayama, *Phys. B*, 2002, **323**, 352–353.
- 20 H. Ma, K. Nakata, L. Pan, K. Hirahara and Y. Nakayama, *Carbon*, 2014, **73**, 71–77.
- 21 P. Kim, L. Shi, A. Majumdar and P. L. Mceuen, *Phys. Rev. Lett.*, 2001, **87**, 215502.
- 22 E. Mayhew and V. Prakash, *Carbon*, 2013, **62**, 493–500.
- 23 H. Ma, L. Pan, Q. Zhao, Z. Zhao and J. Qiu, *Carbon*, 2012, **50**, 778–783.
- 24 J. Zhao, J. Wu, J. W. Jiang, L. Lu, Z. Zhang and T. Rabczuk, *Appl. Phys. Lett.*, 2013, **103**, 635.
- 25 W. Desorbo and W. W. Tyler, *J. Chem. Phys.*, 1953, **21**, 1660–1663.
- 26 T. Yonemura, Y. Suda, H. Tanoue and H. Takikawa, *J. Appl. Phys.*, 2012, **112**, 3919.
- 27 C. Deng, L. Pan, H. Ma and R. Cui, *Carbon*, 2015, **81**, 758–766.
- 28 A. Volodin, M. Ahlskog, E. Seynaeve, H. C. Van, A. Fonseca and J. B. Nagy, *Phys. Rev. Lett.*, 2000, **84**, 3342.
- 29 M. A. Poggi, J. S. Boyles, L. A. Bottomley, A. W. Mcfarland, J. S. Colton, C. V. Nguyen, R. M. Stevens and P. T. Lillehei, *Nano Lett.*, 2004, **4**, 1009–1016.
- 30 K. Hirahara, K. Nakata and Y. Nakayama, *Mater. Sci. Eng., A*, 2014, **595**, 205–212.
- 31 J. Guo, X. Wang and T. Wang, *J. Appl. Phys.*, 2007, **101**, 063537.
- 32 Y. Xie, Z. Xu, S. Xu, Z. Cheng, N. Hashemi, C. Deng and X. Wang, *Nanoscale*, 2015, **7**, 10101.
- 33 J. Liu, W. Qu, Y. Xie, B. Zhu, T. Wang, X. Bai and X. Wang, *Carbon*, 2017, **121**, 35–47.
- 34 J. A. Yan, L. Xian and M. Y. Chou, *Phys. Rev. Lett.*, 2009, **103**, 086802.
- 35 M. J. Matthews, M. A. Pimenta, G. Dresselhaus, M. S. Dresselhaus and M. Endo, *Phys. Rev. B: Condens. Matter Mater. Phys.*, 1999, **59**, R6585–R6588.
- 36 A. J. Bullen, K. E. Ohara, D. G. Cahill, O. Monteiro and A. Von Keudell, *J. Appl. Phys.*, 2000, **88**, 6317–6320.
- 37 M. Shamsa, W. L. Liu, A. A. Balandin, C. Casiraghi, W. I. Milne and A. C. Ferrari, *Appl. Phys. Lett.*, 2006, **89**, 085401.
- 38 Y. M. Sun, C. W. Wang, L. J. Pan, X. Fu, P. H. Yin and H. L. Zou, *Carbon*, 2016, **98**, 285–290.
- 39 A. Matthiessen and C. Vogt, *Philos. Trans. R. Soc. London*, 1864, **154**, 167.
- 40 A. Bulusu and D. G. Walker, *Superlattices Microstruct.*, 2008, **44**.
- 41 B. T. Kelly, *Philos. Mag.*, 1964, **9**, 721–737.